PLANAR FLOW PAST TWO OR MORE BLADES IN GROUND EFFECT

by R. PURVIS *and* F. T. SMITH

(*Mathematics Department, University College London, Gower Street, London* WC1E 6BT)

[Received 9 May 2002. Revise 18 June 2003]

Summary

Planar flow past a finite number of thin blades travelling in sequence, aligned or nearly aligned over flat ground, is examined analytically and numerically for large Reynolds numbers. The work is motivated by concerns with rotorcraft in ground effect. The representative blade length, wake length and height above ground are taken to be comparable, with each wake (except the final one) intersecting the next blade. Inner–outer interaction covers the whole system as all the wake shapes adjust to maintain pressure equality, forcing viscous–inviscid coupling through lateral offsets within each wake. Results are presented for several configurations, in the frame of the blades with the ground moving at freestream speed. The limits of small relative height and of many blades are then investigated. It is found, for the case of identical blade and wake lengths, that as the height is reduced the ground effect first becomes significant at heights just below one half of the blade length but then grows substantially; and that a virtually streamwise periodic motion emerges for about three or more blades.

1. Introduction

Fluid flows induced by a rotor blade have much practical importance, not least with respect to helicopter aerodynamics, as well as in fans, propellers, food mixers, hover mowers and so on. For many years the helicopter has played an important role in both military and civilian air transportation, most crucially when asked to perform tasks that fixed wing aircraft cannot, such as vertical take-off and landing and the capacity to hover. Recent works by Smith and Timoshin (**1**, **2**), Conlisk (**3**), Jones (**4**), Bowles and Smith (**5**, **6**), Bhattacharyya and Smith (**7**) survey the main background in theoretical and numerical terms. When a rotor blade or system is forced to perform near the ground its aerodynamics are considerably altered, with the lift generated for a given power output generally being greatly increased. This is somewhat akin to the ground effect for a single blade or airfoil (see Newman (**8**), Widnall and Barrows (**9**), Tuck and Bentwich (**10**) and references therein, and in particular Jones (**4**) who includes viscous effects as well as inviscid mechanisms considered in earlier articles). In fact, the earliest helicopters were only powerful enough to hover with the assistance of the cushioning effect of the ground. The ground effect has implications in terms of both safety and control of the aircraft as well as providing the opportunity to exploit the phenomenon (see Seddon (**11**), Bramwell (**12**)). There is also relevance to other applications including slip-streaming, pursuit problems, and delay of take-off or landing at airfields (see Moore and Saffman (**13**)). An understanding of how proximity to the ground influences the significant aspects of vorticity shedding from one blade to another and sheltering effects (among others), and the mechanisms by which the enhanced lift is generated, is therefore desirable. However, most

studies are either experimental (see for example Caradonna and Tung (**14**), Parthasarathy *et al.* (**15**), Hoad *et al.* (**16**), Hoad (**17**), Lorber (**18**) and McAlister *et al.* (**19**) among many others), where the very complicated flow structures may mask the underlying physics, or computational (see for example McCroskey (**20**), Egolf and Sparks (**21**), Ramachandran *et al.* (**22**) and Srinivasan and Sankar (**23**)), which generally requires the use of empirical formulae to handle certain features and again important aspects may be lost.

The present theoretical investigation which is motivated by the ground effect on a hovering rotor blade system considers the flow past multiple blades near horizontal ground. As in most of the studies above, modelling for large Reynolds numbers is used, the justification being based on improved analytical and physical understanding in addition to at least qualitative agreement with experiments (Bowles and Smith (**6**)).

The work in effect combines two previous studies in similar regimes. First, Smith and Timoshin (**2**) considered the planar flow past many blades but with no ground effect. An important new interaction is encountered in their article due to non-symmetry, namely inner–outer interaction, whereby the entire viscous-layer and inviscid flows are coupled and must be solved simultaneously. This is discussed below and is of importance in the current regime also. Although we limit ourselves to two-dimensional flow here it still has relevance to the full three-dimensional rotor case in the regime of large radial distance from the hub and that of the many-blade limit, as discussed in Smith and Timoshin (**2**) and Purvis (**24**). Secondly, Jones (**4**) describes the flow past a single blade or aerofoil near the ground. There the author derives a solution for the outer flow given the presence of the ground but has no inner–outer coupling as there is only one blade present. Here we combine these two problems, examining the incompressible flow past many blades in ground effect, and include both the inner–outer interaction aspect and the solving of the inviscid problem for many blades with the ground present. We extend the analysis of Jones (**4**) for the outer flow past a single blade, to find the equivalent relation in the context of flow past many blades, and develop a method to solve it in tandem with the inner viscous-layer flow.

We take as our starting point the steady two-dimensional Navier–Stokes equations in terms of non-dimensional velocity components U, V, corresponding Cartesian coordinates x, y, pressure P and the Reynolds number defined to be $\mathrm{Re} = U_\infty L/\nu$, where ν is the kinematic viscosity of the fluid, U_∞ is the velocity of the free stream and L is a typical length scale, taken here as the length of a representative blade. The freestream pressure is written as P_∞. For Re large the motion is expected to split into viscous and inviscid parts. The configuration of the problem is that of n thin blades, the ith one running from its leading edge $x = a_i$ to its trailing edge $x = b_i$. The blade shapes are given by $y = \mathrm{Re}^{-\frac{1}{2}} f^{\pm}(x)$, where $f^+(x)$, $f^-(x)$ give the upper and lower blade shapes respectively and are assumed to be smooth and typically $O(1)$. We also require that $f^+(x) = f^-(x)$ at the leading and trailing edges. These blades are positioned in a slip-streaming arrangement at an $O(1)$ distance h above the moving ground and in an otherwise uniform stream with non-dimensional velocity of unity. We take the first leading edge a_1 to be the origin. Thus the coordinate frame has the blades being fixed, while the ground moves horizontally with velocity 1; see Fig. 1.

In section 2 the two parts of the problem are examined, both the viscous layer's multi-blade flow (section 2.1) and the outer inviscid flow (section 2.2) driven by displacement effects from the viscous layer(s). We also discuss in more detail the all-important inner–outer interactions introduced above. Having set up the outer problem in terms of needing to find an analytic function in the complex plane, we turn in section 2.2 to solving the inviscid problem, determining integral equations for the velocity and pressure, and then solve these to enable calculation of the unknown outer flow in terms

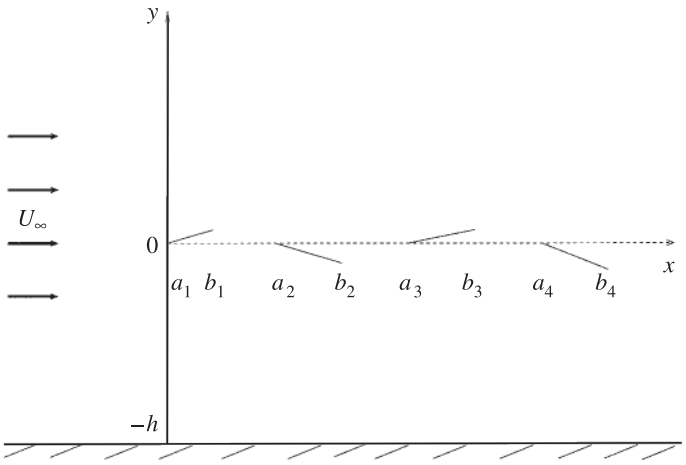

Fig. 1 The flow configuration of $n(= 4$ here) blades at a distance h above horizontal moving ground. Although shown as flat plates here they can have thickness and a shape through $f(x)$

of the unknown inner. We move in section 3 to consider the numerical solution of the combined inner and outer problem. Results are presented in section 4 for several configurations, varying the number, the ground clearance and angle of attack of the blades. The computational results are then used to guide further analysis. In section 5 we consider two limits of interest, those of large and small ground clearances h. For large clearances, we derive an expression for the leading-order ground effect, recovering the no ground effect case of Smith and Timoshin (**2**). In the case of small h a relatively simple form for the pressure and velocities emerges, yielding good agreement with the relevant results from section 4. Then section 6 addresses the many-blade limit (large n), in which a periodic flow forms on each blade and wake, accompanied by slower variation over a long length scale. Further comments are made in section 7.

2. Flow structure

2.1 *The viscous layers*

With Re being large, the aim as far as the viscous part of the motion is concerned is to resolve the viscous boundary-layer and wake motions for the flow past all the blades. Although the ground is outside the viscous layers, the effect of the ground does enter through the necessary coupling of the solution for the boundary layer and wake with properties from the outer inviscid flow by means of unknown lateral shifts in the wake shapes at each leading edge, developed in more detail below.

We introduce the scaled viscous coordinate Y in the normal direction given by $y = \mathrm{Re}^{-\frac{1}{2}}[f(x) + Y]$, where $f(x)$ is the scaled shape of the known blade and unknown wake centre-line. The governing equations then become, for the scaled velocity components $\bar{u}[= U]$, $\bar{v}[\equiv \mathrm{Re}^{\frac{1}{2}} V - \bar{u} f'(x)]$,

$$\frac{\partial \bar{u}}{\partial x} + \frac{\partial \bar{v}}{\partial Y} = 0, \quad \bar{u}\frac{\partial \bar{u}}{\partial x} + \bar{v}\frac{\partial \bar{u}}{\partial Y} = 0 + \frac{\partial^2 \bar{u}}{\partial Y^2}, \tag{2.1a,b}$$

subject to the no-slip and free-stream conditions

$$\bar{u} = \bar{v} = 0 \quad \text{at} \quad Y = 0 \quad \text{on each blade,} \tag{2.1c}$$

$$\bar{u} \to 1 \quad \text{as} \quad Y \to \pm\infty, \tag{2.1d}$$

in turn, with the velocities being continuous in the wakes. There is also a starting condition at the first leading edge requiring

$$\bar{u} = 1 \quad \text{at} \quad x = 0, \quad Y \neq 0. \tag{2.1e}$$

The Prandtl transposition used above is known on the blades, with $f(x) = f^{\pm}(x)$, but is unknown in the wakes as the wake centre-line shape is to be found. With a single aerofoil this does not affect the boundary-layer calculation; there is Blasius flow over the aerofoil and a Goldstein-type wake beyond the trailing edge, regardless of the wake shape which can then be obtained independently by examining the outer flow. By contrast, in the present multi-blade case the wake shape is crucial. If the position of the wake centre-line as the wake encounters the following blade is unknown, that is, the position of the leading edge in relation to the oncoming flow is unknown, then the flow solution in the subsequent boundary layer cannot be determined. The Y-shift in each wake flow, the scaled distance by which each wake centre-line is deflected at the onset of the next leading edge, is determined by considering the outer flow introduced in the next subsection. Likewise the outer inviscid flow, driven by the presence of the viscous layers, cannot be calculated until the boundary layer(s) and wake(s) and hence the scaled displacement effects,

$$\delta_{\pm}(x) \equiv \pm \int_0^{\pm\infty} (1 - \bar{u}(x, Y))dY, \tag{2.2}$$

which drive the outer flow, have been resolved. This causes inner–outer interaction, with each aspect (viscous, inviscid) of the overall problem requiring the solution to the other.

2.2 *The outer inviscid parts*

Outside the boundary layer the free stream $U = 1$ is only slightly disturbed by the presence of the sequence of thin blades and related viscous layers and hence we expand the velocities and pressure as

$$U = 1 + \epsilon v(x, y) + \cdots, \qquad V = 0 + \epsilon v(x, y) + \cdots, \qquad P = P_\infty + \epsilon p(x, y) + \cdots, \tag{2.3a,b,c}$$

where $\epsilon \equiv \mathrm{Re}^{-\frac{1}{2}}$ is small. So the Euler equations hold but linearized about the free stream, yielding the Cauchy–Riemann equations for v and p. We express the flow problem here in terms of the complex function $w(x + iy) = p(x, y) + iv(x, y)$ which is analytic and required to be bounded in the far field, and we define

$$\begin{aligned} w(x + 0i) &= p_+(x) + iv_+(x), \\ w(x - 0i) &= p_-(x) + iv_-(x), \\ w(x - hi) &= p_=(x) + i0 \end{aligned} \tag{2.4a,b,c}$$

as the pressures and velocities just above and below the viscous layers, and the pressure on the ground, respectively. The boundary condition at the ground is $v_= = 0$ in view of the negligible viscous displacement produced by the horizontal movement there. We also impose pressure continuity across the wake which requires

$$p_+(x) = p_-(x) \quad \text{in the wakes.} \tag{2.4d}$$

This condition is required since the largest pressure jump that each wake can support is typically $O(\mathrm{Re}^{-1})$ at most.

The outer flow is driven by displacement effects from the viscous layers, so that matching requires

$$v_\pm = \begin{cases} s'(x) & \text{for } x < 0, \\ c'(x) \pm \frac{1}{2}t'(x) \pm \delta'_\pm(x) & \text{for } x \text{ on blades,} \\ s'(x) \pm \delta'_\pm(x) & \text{for } x \text{ in wakes,} \end{cases} \tag{2.5}$$

where $\epsilon c(x) = \epsilon(f^+(x) + f^-(x))/2$ is the camber of the blade, $\epsilon t(x) = \epsilon(f^+(x) - f^-(x))$ is the thickness of the blade, $\epsilon s(x)$ is the wake centre-line shape and $\delta_\pm(x)$ are the viscous displacement thicknesses given by (2.2). For given blade shapes, $c(x)$ and $t(x)$ are known while $s(x)$ is unknown and must be determined as part of the whole inviscid solution. Also, $\delta_\pm(x)$ can be determined from the viscous layers through (2.2) only once $s(x)$, and hence the Y-shifts, are computed.

In the inviscid problem, to satisfy the ground condition (2.4c), we introduce the image of the system of blades at $y = -2h$. This requires finding the analytic complex function w bounded in the far field but now satisfying

$$w(x \pm 0i) = p_\pm(x) + i v_\pm(x), \tag{2.6a}$$

$$w(x - 2hi \pm 0i) = p_\mp(x) - i v_\mp(x), \tag{2.6b}$$

$$p_+(x) = p_-(x) \quad \text{in the wakes.} \tag{2.6c}$$

Following the method employed by Jones (**4**) for a single blade, we apply Cauchy's integral formula for w using the contours $\Gamma_+, \Gamma_=, \Gamma_-$ in the complex plane as in Fig. 2 at a point away from $y = 0$, and in the limit as the radius R of the semi-circles in $\Gamma_\pm$ tends to infinity we find

$$w(z) = \frac{1}{2\pi i}\int_{-\infty}^{\infty} \frac{[p](\xi) + i[v](\xi)}{\xi - z} d\xi - \frac{1}{2\pi i}\int_{-\infty}^{\infty} \frac{[p](\xi) - i[v](\xi)}{\xi - 2ih - z} d\xi. \tag{2.7a}$$

Here and in what follows we use the notation

$$[v](x) = v_+(x) - v_-(x), \quad \langle v\rangle(x) = v_+(x) + v_-(x), \tag{2.7b,c}$$

and so on for the differences and sums of the velocities and pressures on each side of the viscous layer. The real and imaginary parts of (2.7a) give the pressure and normal velocity as

$$p(x,y) = \frac{1}{2\pi}\int_{-\infty}^{\infty} \left(\frac{\xi - x}{(\xi - x)^2 + y^2} + \frac{\xi - x}{(\xi - x)^2 + (y + 2h)^2} \right) [v](\xi) d\xi$$
$$+ \frac{1}{2\pi}\int_{-\infty}^{\infty} \left(\frac{y}{(\xi - x)^2 + y^2} - \frac{y + 2h}{(\xi - x)^2 + (y + 2h)^2} \right) [p](\xi) d\xi, \tag{2.8a}$$

$$v(x,y) = \frac{1}{2\pi}\int_{-\infty}^{\infty} \left(\frac{y}{(\xi - x)^2 + y^2} + \frac{y + 2h}{(\xi - x)^2 + (y + 2h)^2} \right) [v](\xi) d\xi$$
$$- \frac{1}{2\pi}\int_{-\infty}^{\infty} \left(\frac{\xi - x}{(\xi - x)^2 + y^2} - \frac{\xi - x}{(\xi - x)^2 + (y + 2h)^2} \right) [p](\xi) d\xi, \tag{2.8b}$$

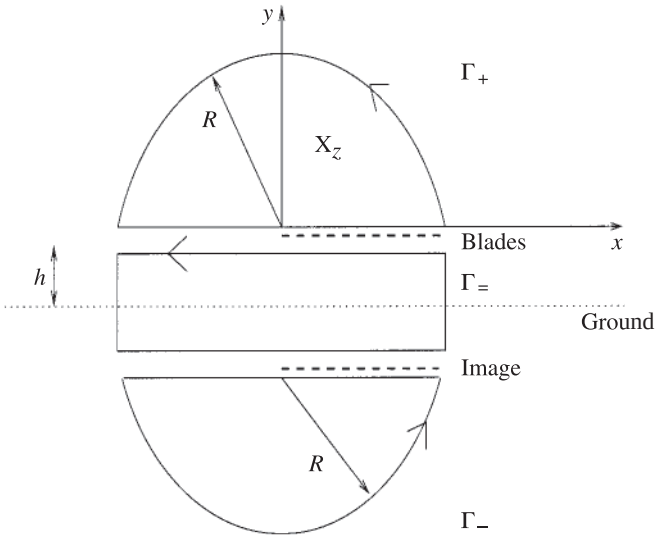

Fig. 2 Contours Γ_+, $\Gamma_=$ and Γ_- for a point away from $y = 0$

and then $u\ (= -p)$ follows. However, while $[p](x)$ is known to be zero in the wakes from (2.6c), the pressure difference is unknown on the blades. To determine the outer solution we must determine $[p](x)$ for all x. For this we again use Cauchy's integral formula but this time at a point on $y = 0$ and use the new contours Γ_+, $\Gamma_=$, Γ_-, where Γ_+, $\Gamma_=$ now circumnavigate the point x with a small semi-circle of radius ϵ. In the limit as $R \to \infty$ and $\epsilon \to 0$ we obtain

$$w(x+0i) + w(x-0i) = \frac{1}{\pi i}\int_{-\infty}^{\infty} \frac{w(\xi+0i) - w(\xi-0i)}{\xi - x} d\xi - \frac{1}{\pi i}\int_{-\infty}^{\infty} \frac{w(\xi - 2hi + 0i) - w(\xi - 2hi - 0i)}{\xi - x - 2hi} d\xi. \tag{2.9}$$

Applying the boundary conditions (2.6a,b) gives, from the real and imaginary parts, the integral relations

$$\langle v \rangle = \frac{1}{\pi}\int_{-\infty}^{\infty} l(\xi - x)[v](\xi) d\xi - \frac{1}{\pi}\int_{-\infty}^{\infty} \left(\frac{1}{\xi - x} - m(\xi - x)\right)[p](\xi) d\xi, \tag{2.10a}$$

$$\langle p \rangle = \frac{1}{\pi}\int_{-\infty}^{\infty} \left(\frac{1}{\xi - x} + m(\xi - x)\right)[v](\xi) d\xi - \frac{1}{\pi}\int_{-\infty}^{\infty} l(\xi - x)[p](\xi) d\xi, \tag{2.10b}$$

where $l(x) = \dfrac{2h}{x^2 + 4h^2}$, $m(x) = \dfrac{x}{x^2 + 4h^2}$. The integral equations (2.10) for the velocity and pressure sums must be solved subject to the boundary conditions

$$[v](x) = \begin{cases} 0 & \text{for } x < 0, \\ t'(x) + (\delta'_+ + \delta'_-)(x) & \text{on blades,} \\ (\delta'_+ + \delta'_-)(x) & \text{in the wakes,} \end{cases} \tag{2.11a}$$

$$\langle v\rangle(x) = 2c'(x) + (\delta'_+ - \delta'_-)(x) \text{ on blades,} \tag{2.11b}$$

$$[p](x) = 0 \text{ in the wakes,} \tag{2.11c}$$

from (2.4d), (2.5), with the quantities $\langle v\rangle, \langle p\rangle$ in the wakes and $[p], \langle p\rangle$ on the blades being unknown, to be determined from solving (2.10a,b). Possibly the most significant quantity is $\langle v\rangle(x) = 2s'(x) + (\delta'_+ - \delta'_-)(x)$ in the wakes, which will allow us to find the Y-shifts required in the viscous-layer calculation later. However, while $[v](x)$ is known for all x through (2.11a), we cannot determine $\langle v\rangle(x)$ until we obtain $[P](x)$ on the blades. Once we have $[p](x)$ everything else follows from (2.10), (2.11) along with the simple relation $2v_\pm(x) = \langle v\rangle(x) \pm [v](x)$ and similarly for p.

After a slight rearrangement (2.10a) becomes

$$\frac{1}{\pi}\int_{\text{blades}} \left(\frac{1}{\xi - x} - m(\xi - x)\right)[p](\xi)d\xi = \frac{1}{\pi}\int_{-\infty}^{\infty} l(\xi - x)[v](\xi)d\xi \; - \langle v\rangle(x), \tag{2.12a}$$

where

$$\int_{\text{blades}} \equiv \sum_{i=1}^{n}\int_{a_i}^{b_i}, \tag{2.12b}$$

since $[p](x) = 0$ in the wakes. The above is a singular Fredholm equation of the first kind for $[p](x)$, where the right-hand side can be calculated from the viscous-layer calculation and the boundary conditions (2.11a,b). This type of integral equation, notoriously difficult to solve, can be reduced to one of the second kind. It has a Cauchy kernel. We rewrite (2.12a) as

$$\frac{1}{\pi}\int_{\text{blades}} \frac{[p](\xi)}{\xi - x}d\xi = f(x) + \frac{1}{\pi}\int_{\text{blades}} m(\xi - x)[p](\xi)d\xi, \tag{2.13a}$$

where

$$f(x) = \frac{1}{\pi}\int_{-\infty}^{\infty} l(\xi - x)[v](\xi)d\xi - \langle v\rangle(x). \tag{2.13b}$$

Then applying a result from Muskhelishvili (**25**) to (2.13a) we obtain

$$\psi(x) = h(x) + \frac{1}{\pi}\int_{\text{blades}} S^{-\frac{1}{2}}(\xi)M(x,\xi)\psi(\xi)d\xi, \tag{2.14a}$$

where

$$h(x) = -\frac{1}{\pi}\int_{\text{blades}} \frac{S^{\frac{1}{2}}(\xi)f(\xi)}{\xi - x}d\xi, \qquad M(x,\xi) = -\frac{1}{\pi}\int_{\text{blades}} \frac{S^{\frac{1}{2}}(\xi_1)m(\xi_1 - \xi)}{\xi_1 - x}d\xi_1, \tag{2.14b,c}$$

and

$$\psi(x) = S^{\frac{1}{2}}(x)[p](x), \quad S(x) = \prod_{i=1}^{n}\left|\frac{x - a_i}{x - b_i}\right|. \tag{2.14d,e}$$

Here (2.14a), which is a Fredholm equation of the second kind, determines, via (2.14d,e), the required pressure differences on the blades.

3. Numerical method

For the viscous-layer calculations we adopted a semi-explicit finite-difference approach of second-order accuracy as in Smith and Timoshin (**1**, **2**), which is robust, accurate and has little difficulty in dealing with the leading and trailing edge irregularities present in the multi-blade flows. The momentum equation (2.1b) is discretized as

$$\bar{u}_{i-1j}\frac{\bar{u}_{ij}-\bar{u}_{i-1j}}{\Delta_x}+\bar{v}_{i-1j}\frac{\bar{u}_{ij+1}-\bar{u}_{ij-1}}{2\Delta_Y}=\frac{\bar{u}_{ij+1}-2\bar{u}_{ij}+\bar{u}_{ij-1}}{\Delta_Y^2}, \tag{3.1}$$

where $\bar{u}_{ij}$ ($j=-J$ to J) are the unknown $\bar{u}$ quantities at the x-station $i\Delta_x$, for Y values $j\Delta_Y$, with step sizes Δ_x, Δ_Y in the x and Y directions respectively. Along with the relevant boundary conditions from (2.1c,d), this determines all of the required $\bar{u}_{ij}$ values at the current station. The continuity equation (2.1a) is discretized similarly as

$$\frac{\bar{u}_{ij}-\bar{u}_{i-1j}}{\Delta_x}=-\frac{\bar{v}_{ij+1}-\bar{v}_{ij-1}}{2\Delta_Y}, \tag{3.2}$$

allowing the $\bar{v}_{ij}$ values to be determined at any given x-station once the $\bar{u}_{ij}$ have been calculated from (3.1).

These discretizations are second-order accurate in Y but as yet only first-order accurate in x. Second-order x-accuracy is obtained by employing a double-stepping procedure (Smith and Timoshin (**1**,**2**)). Further, at each of the x-stations $a_i-\Delta_x$ a careful interpolation of the approaching flow profile is necessary in order to have the correct profile to integrate over the ith blade. Rather than just sweeping as before at these points we know the leading edge to be at the point $Y=f^+(a_i)$ and we re-align the oncoming profiles of $\bar{u}_{i-1j}$ and $\bar{v}_{i-1j}$, interpolating them using cubic splines and then shifting them up or down by the relevant distance calculated/updated through the inviscid region. This is how the ground effect, via the inviscid problem, permeates the viscous-layer calculation. Typically $\Delta_x=0{\cdot}005$, $\Delta_y=0{\cdot}05$ and $J=400$ were found to be sufficient to obtain accuracy to within $O(10^{-6})$ except perhaps far downstream with many blades present.

There are several parts to determining the outer contribution ψ. We limit our discussion to blades of unit length, that is, we take $b_i-a_i=1$, and also to gaps of unit length, that is, $a_i-b_{i-1}=1$, to illustrate the method of solution, and the solutions themselves, without excessive complication.

First for the calculation of (2.14b) we introduce $\hat{S}_j(x)$ such that

$$\left|\frac{x-a_j}{x-b_j}\right|\hat{S}_j(x)=S(x),\qquad h(x)=-\frac{1}{\pi}\int_{\text{blades}}\left|\frac{\xi-a_j}{\xi-b_j}\right|^{\frac{1}{2}}\frac{\hat{S}_j^{\frac{1}{2}}(\xi)\,f(\xi)}{\xi-x}d\xi. \tag{3.3a,b}$$

There are two problems to be addressed here: on each blade the integral has a square root singularity at $\xi=b_i$ and, if x is on the blade, also a Cauchy-type kernel. For the former we make the substitution $\xi=b_j-\cos^2\theta=\sin^2\theta+a_j$, $x=\sin^2\phi+a_i$. Substituting into (3.3b) gives

$$h(\sin^2\phi+a_i)=-\frac{2}{\pi}\sum_{j=1,\,j\neq i}^{j=n}\int_0^{\pi/2}\frac{\sin^2\theta\,\hat{S}_j^{\frac{1}{2}}(\sin^2\theta+a_j)\,f(\sin^2\theta+a_j)}{\sin(\theta+\phi)\sin(\theta-\phi)+(a_j-a_i)}d\theta$$

$$-\frac{2}{\pi}\int_0^{\pi/2}\frac{\sin^2\theta\,\hat{S}_j^{\frac{1}{2}}(\sin^2\theta+a_j)(\theta-\phi)}{\sin(\theta+\phi)\sin(\theta-\phi)}\frac{f(\sin^2\theta+a_j)}{(\theta-\phi)}d\theta, \tag{3.4}$$

where the integrals in the summation are no longer singular and the final one is now a Cauchy integral. The former are straightforward to evaluate numerically. To calculate the final one we used a NAG library routine D01AQF, as the non-Cauchy part of that final one is no longer singular. Similar substitutions are made for the calculation of M. To solve (2.14a) we adopted a simple iteration procedure,

$$\psi_{k+1}(\sin^2\phi + a_i) = h(\sin^2\phi + a_i) + \frac{2}{\pi}\int_{\text{blades}} S^{-\frac{1}{2}}(\sin^2\theta + a_j)M(\sin^2\phi + a_i, \sin^2\theta + a_j)\psi_k(\theta)\sin\theta\cos\theta d\theta, \tag{3.5}$$

from an initial guess ψ_0. Typically to obtain convergence such that $|\psi_{k+1} - \psi_k| \sim O(10^{-6})$ required about one hundred iterations of (3.5).

Finally updated values of the Y-shifts at each leading edge are found through (2.11). Since in the wake $v_\pm = s'(x) \pm \delta'_\pm(x)$, integration with respect to x in the wake between blades i and $i+1$ gives the wake shape as

$$s(x) = s(b_i) + \frac{1}{2}\int_{b_i}^{x} \{\langle v\rangle(\xi) - (\delta'_+(\xi) - \delta'_-(\xi))\}d\xi, \tag{3.6a}$$

and hence the Y-shift $Y_s(a_{i+1})$ at the leading edge of blade $i+1$ is

$$Y_s(a_{i+1}) = s(b_i) + \frac{1}{2}\int_{b_i}^{a_{i+1}} \{\langle v\rangle(\xi) - (\delta'_+(\xi) - \delta'_-(\xi))\}d\xi, \tag{3.6b}$$

where $s(b_i)$ is known from the position of the previous trailing edge, $\langle v\rangle(x)$ is calculated from (2.10a) and $\delta'_\pm(x)$ from the viscous-layer calculations. Working with δ' is convenient as it is given by the value of the lateral velocity at the edge of the viscous layer.

In summary, the sweeping used to determine the complete viscous-layer and inviscid flows is as follows.

1. Make an initial guess for the Y-shift at each leading edge; typically $Y_s(a_j) = 0$ for all j is a sufficiently good first estimate.
2. Sweep through the viscous-layer solution, interpolating where necessary to satisfy the current Y-shift guesses.
3. Compute $\delta'_\pm(x)$, and hence $[v](x)$, using (2.2) and the viscous-layer solution.
4. Calculate $[p](x)$ by iterating on (2.14a), calculating $f(x)$ from the new $[v](x)$ values.
5. Using the $[p](x)$ values, calculate $\langle v\rangle(x)$ through (2.10a) and hence recalculate new Y-shift approximations from (3.6b).
6. Check on convergence; return to 2 and re-sweep, or finish.

Depending on the configuration, this procedure typically takes four to eight complete cycles for an accuracy of the order 10^{-6} in successive Y-shift approximations.

Evaluating $\psi(\sin^2\phi + a_i)$ was found to require a step size in ϕ of about $\pi/500$ to obtain the same order of accuracy. All of the results were checked by varying the grid sizes to ensure numerical accuracy.

4. Results

Results are presented in Figs 3 to 9 for various flow geometries, varying the number of blades, the blade height h and the angle of attack through $c(x)$. These figures show the viscous displacement

thicknesses $\delta_{\pm}(x)$, wake shapes $s(x)$ and the pressures $p_{\pm}$, $p_{=}$. We consider mainly two different configurations in detail, presenting results for two and five blades (later nine blades are examined briefly), varying h and considering three sample cases: that of flat blades and two examples of non-symmetry where the blades have positive and then negative angle of attack. In the case of five flat plates, each with zero camber and thickness, Figs 3a and 3b show the displacement thicknesses and Figs 4a and 4b show the pressures for a variety of heights ranging from $h = 4$ to $h = \frac{1}{32}$. There is very little variation in the pressures with varying h for values of $h > \frac{1}{2}$. As h is decreased p_{-} increases rapidly while p_{+} is relatively unchanged. Closer inspection of the small-h cases suggests p_{-} increasing like $1/h$, an extreme which is explored further in the next section. Another striking feature of the small-h cases is the very flat shapes in the lower displacement thicknesses in the wake. Physically this is due to the pressure requirement causing relatively little fluid to be entrained from beneath the wake compared with that above and forcing the downward reflection of $s(x)$. The flow appears to have a relatively simple form here and we examine it in more detail in section 5. There also appear to be distinct leading and trailing edge regions, similar to those considered by Jones (**4**), where the wake shape and the pressure adjust rapidly. We also present in Figs 5a,b a few examples of the displacement thicknesses for five blades at positive and negative angles of attack. Features analogous to those discussed earlier can be observed.

In Figs 6a,b we present the corresponding results for two flat blades, seeing features similar to those of the five-blade case.

Figures 7a,b give the case of two blades at an angle of attack with $c(x)$ no longer zero, considering in turn both positive and negative angles. Similar features are again observed, with the flattening wake shape and increasing pressure differences $[p]$ as h is reduced still clearly visible. Other configurations of possible interest include having each blade with a different camber and also experimenting with varying the thickness of the blades, but these are not featured here.

In Fig. 8 we present the lift profiles, from the integrals of the pressure differences $[p](x)$ along each blade, for the five-flat-blade case at each of the values of h considered. Away from the ground this configuration does not normally generate any lift; so any lift here is solely as a direct result of the influence of the ground. For the larger h values (greater than one-half) there is effectively no lift generated. As h is reduced, and there is a non-zero lift produced, sheltering effects are clearly visible, with more lift created on the first blade compared with the following ones. The lift can be seen to increase substantially as $1/h$ as h is reduced even further.

Finally here, we also present a single case of nine blades, at a height $h = \frac{1}{32}$, in Fig. 9. Observe the almost periodic nature of the wake shape beyond the third or fourth blade and the similar $\delta_{\pm}(x)$ shapes, except for the gradual growth. This suggests there are two important length scales present: one shorter scale from leading edge to successive leading edge with a fast-varying and periodic form, and a longer slowly varying scale containing the steady growth in size of the boundary layer. This is considered in more detail in section 6.

5. Extreme clearances

5.1 *Large ground clearances* ($h \gg 1$)

When the distance between the blades and the ground is large, the velocity and pressure sums and differences expand as

$$\langle v\rangle(x) = \langle v\rangle_0(x) + \frac{1}{2h}\langle v\rangle_1(x) + \cdots, \qquad [v](x) = [v]_0(x) + \frac{1}{2h}[v]_1(x) + \cdots \tag{5.1}$$

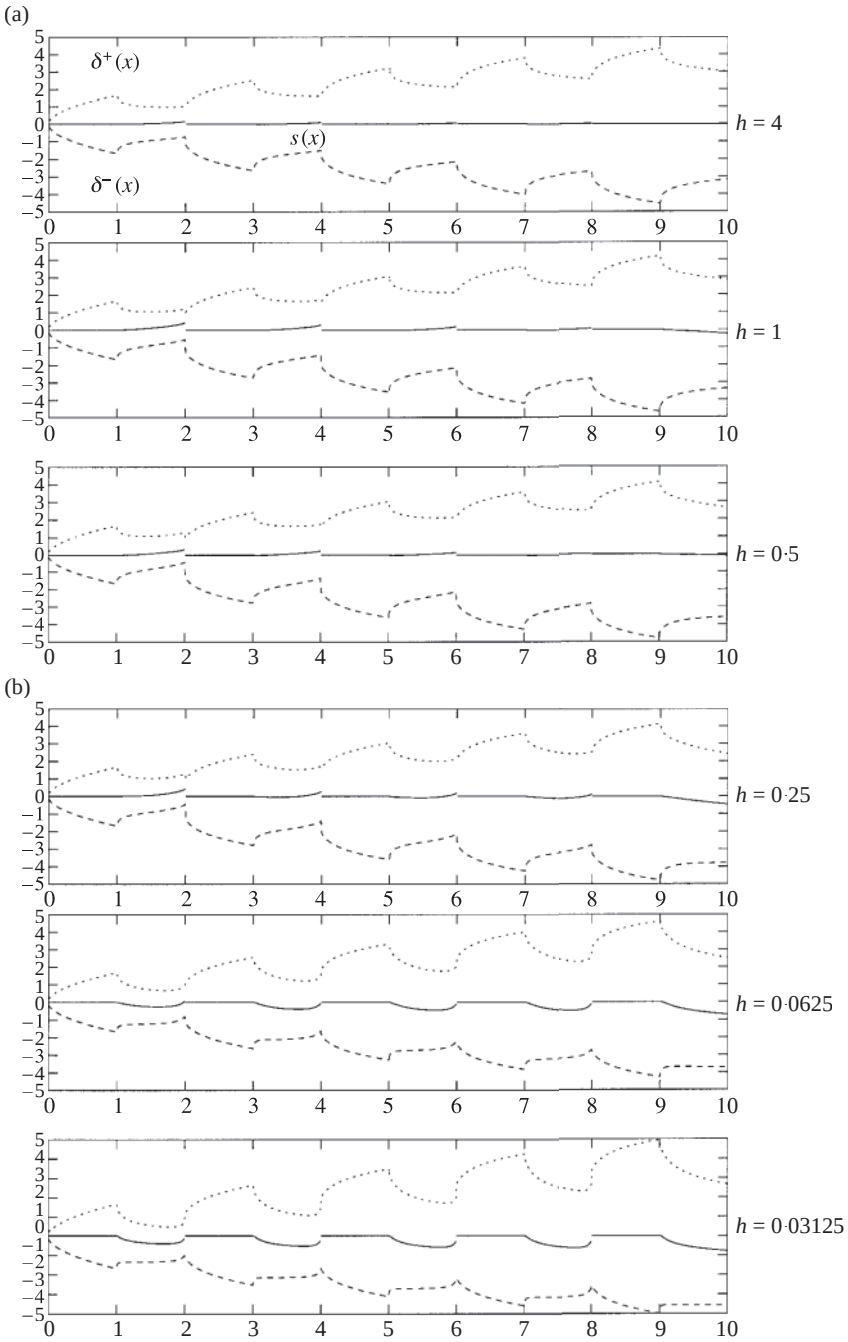

Fig. 3 Displacement thicknesses $\delta_{\pm}(x)$ and wake shapes $s(x)$ for five flat blades at heights (a) from $h = 4$ to $h = \frac{1}{2}$, (b) from $\frac{1}{4}$ to $\frac{1}{32}$

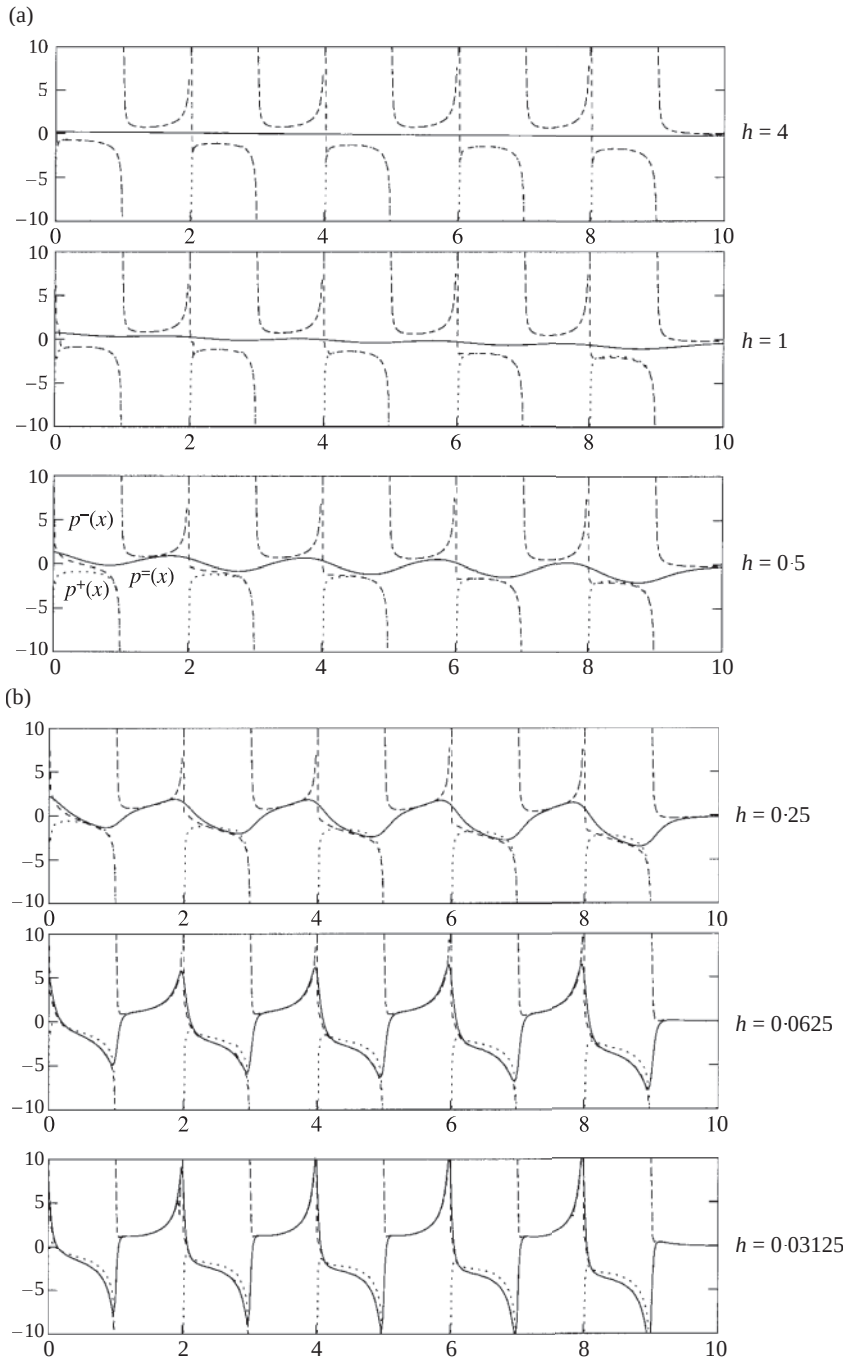

Fig. 4 Plots of the above, below and ground pressures $p_+(x)$, $p_-(x)$ and $p_=(x)$, for the case of five flat blades, with h values ranging (a) from $h = 4$ to $h = \frac{1}{2}$, (b) from $\frac{1}{4}$ to $\frac{1}{32}$

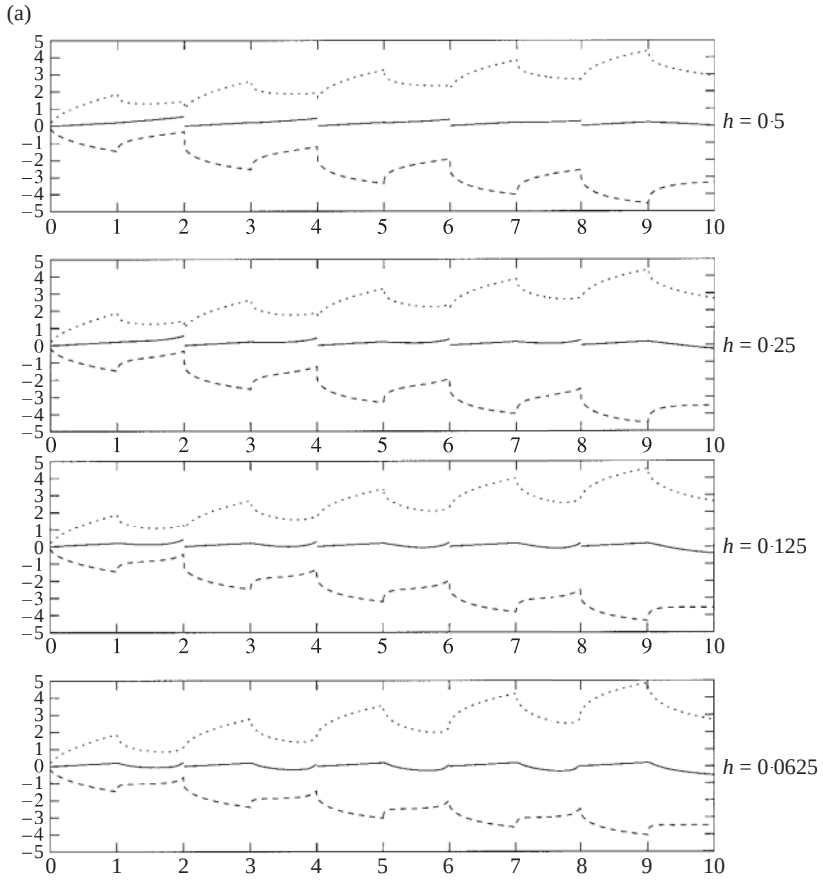

Fig. 5 Displacement thicknesses and wake centre-line shapes for five blades at angle of attack, for various heights; (a) positive angle

and so on, together with expansions of $\ell(x)$, $m(x)$ for $x \ll h$. Care must be taken when $x \sim h \gg 1$ to ensure that all the necessary terms are retained at each order. Substituting into (2.10) yields, to leading order,

$$\langle v\rangle_0 = -\frac{1}{\pi}\int_{-\infty}^{\infty} \frac{[p]_0(\xi)}{\xi - x}d\xi, \qquad \langle p\rangle_0 = \frac{1}{\pi}\int_{-\infty}^{\infty} \frac{[v]_0(\xi)}{\xi - x}d\xi. \tag{5.2}$$

These can be inverted readily to give

$$[p]_0(x) = \frac{S^{-\frac{1}{2}}(x)}{\pi}\int_{\text{blades}} \frac{S^{\frac{1}{2}}(\xi)}{\xi - x}\langle v\rangle_0(\xi)d\xi, \tag{5.3}$$

as in Smith and Timoshin (**2**) for the flow past multiple blades with no ground present. The entire leading-order solution can now be calculated as before. To next order, and including the

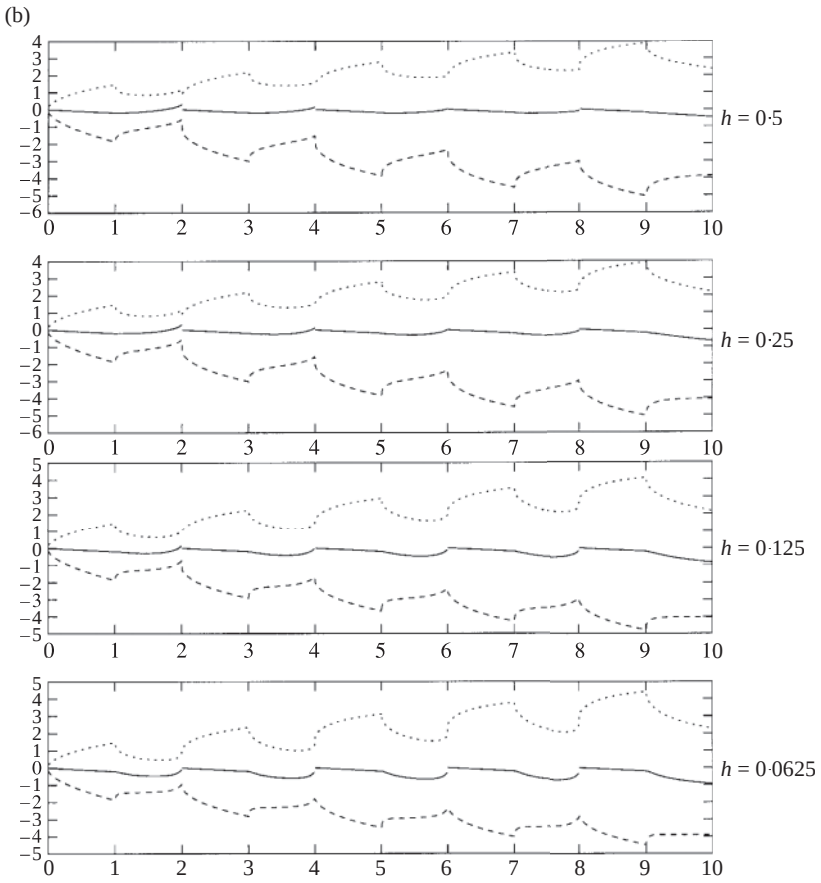

Fig. 5 cont. (b) negative angle

contributions from the region where $\xi \sim h$ (Purvis (**24**)), we obtain the complete expressions as

$$\langle v\rangle_1 = \frac{1}{\pi}\int_{-\infty}^{\infty}([v]_1 - \langle v\rangle_0)(\xi)d\xi - \frac{1}{\pi}\int_{-\infty}^{\infty}\frac{[p]_1(\xi)}{\xi - x}d\xi, \tag{5.4a}$$

$$\langle p\rangle_1 = -\frac{1}{\pi}\int_{-\infty}^{\infty}([p]_1 - \langle p\rangle_0)(\xi)d\xi + \frac{1}{\pi}\int_{-\infty}^{\infty}\frac{[v]_1(\xi)}{\xi - x}d\xi. \tag{5.4b}$$

These can also be inverted to yield an expression for $[p](x)$ on the blades and hence give the complete solution; (5.4) provide the first sign of the effect of the ground as the $O(1/2h)$ correction is the leading-order ground effect for large h. Notice also that the first integrals in (5.4) are dependent only upon the quantities beneath the blades, v_- and p_- respectively.

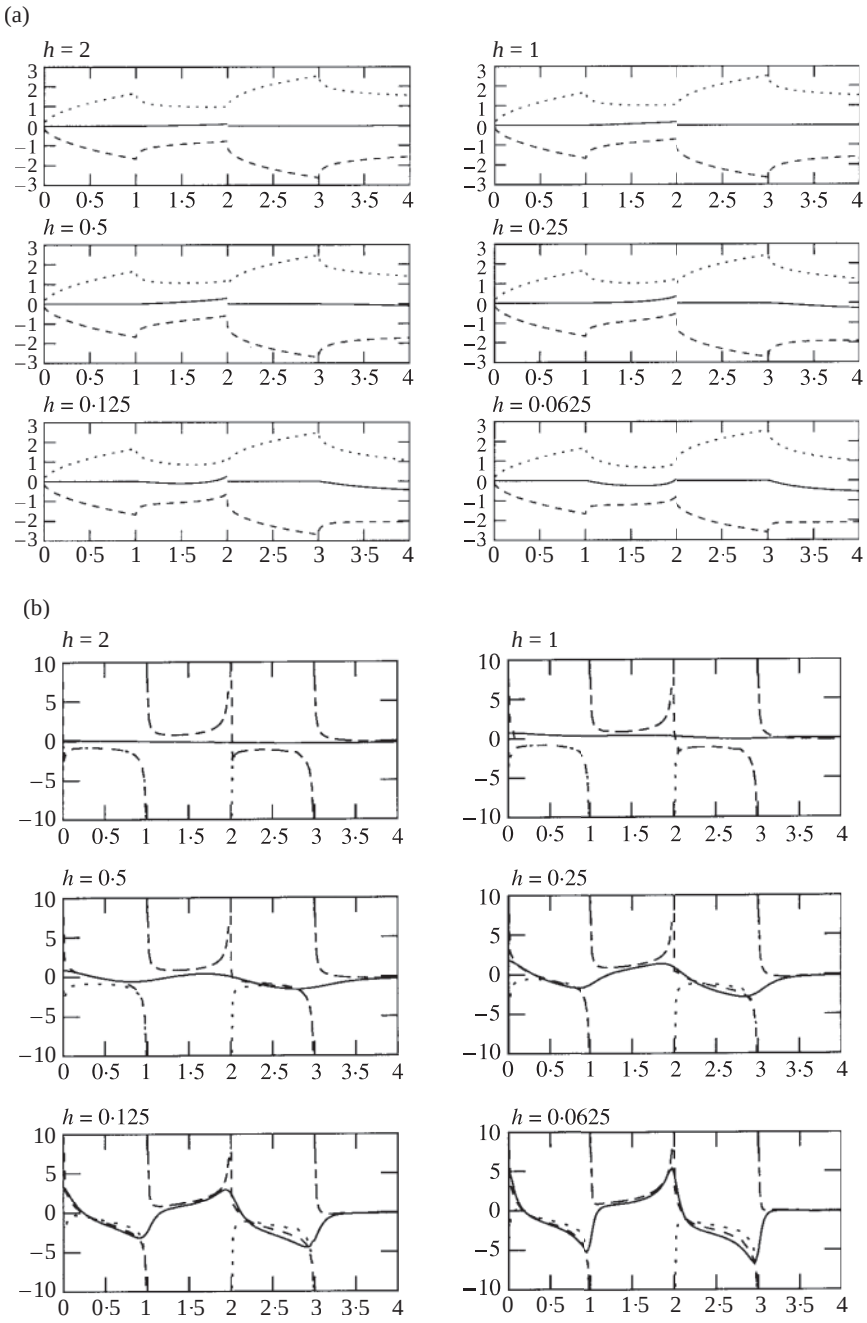

Fig. 6 For two flat blades, (a) displacement thicknesses $\delta_{\pm}(x)$ and wake shapes $s(x)$, (b) pressures $p_{=}$ (solid line), p_{+} (dotted line) and p_{-} (dashed line)

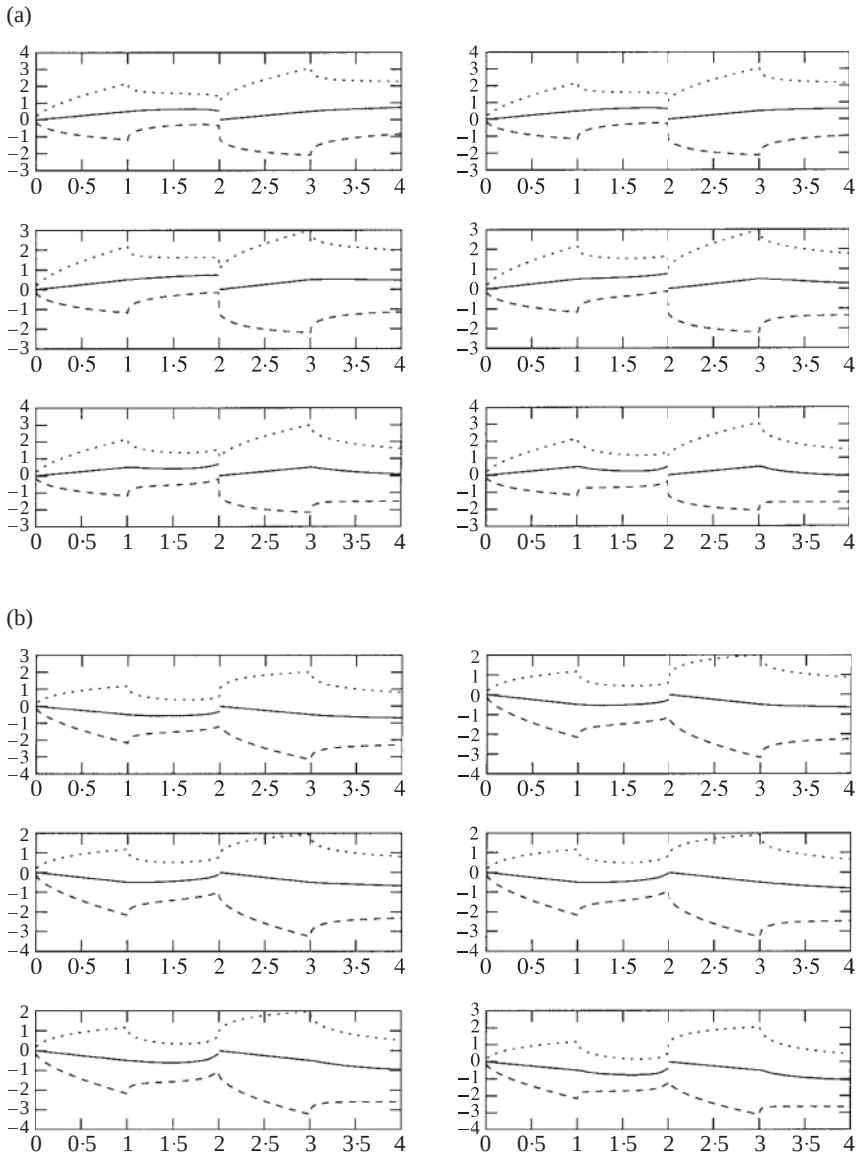

Fig. 7 Displacement thicknesses $\delta_{\pm}(x)$ and wake shapes $s(x)$ for two blades at angle of attack for heights $h = 2$ to $h = 0{\cdot}0625$ as in Fig. 6a; (a) positive, (b) negative angle

5.2 *Small ground clearances* ($h \ll 1$)

For the other extreme, of small ground clearances, although still sufficiently large that the ground is entirely outside the viscous layers, we return to the original Cauchy–Riemann equations for v and p. (See also Jones (**4**) who uses a different approach for a single blade.) We write $y + h = h\hat{y}$ and

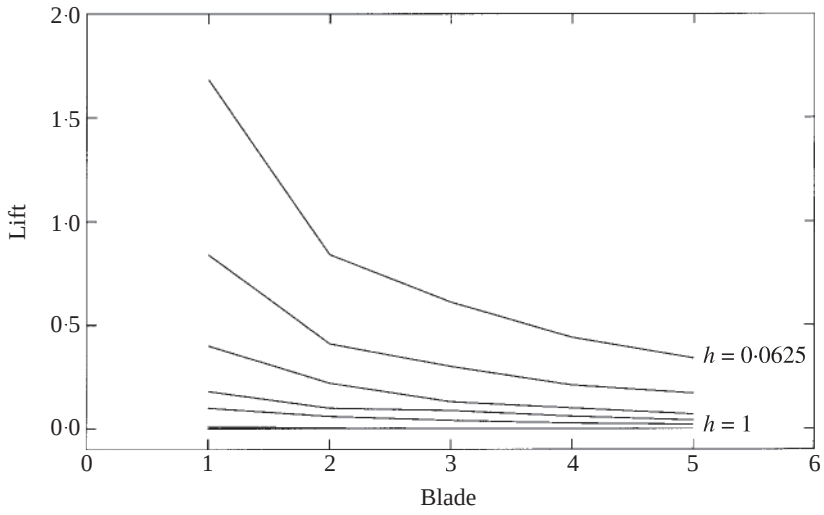

Fig. 8 Scaled lift on each of the five flat blades for the various heights presented in Figs 3 to 5

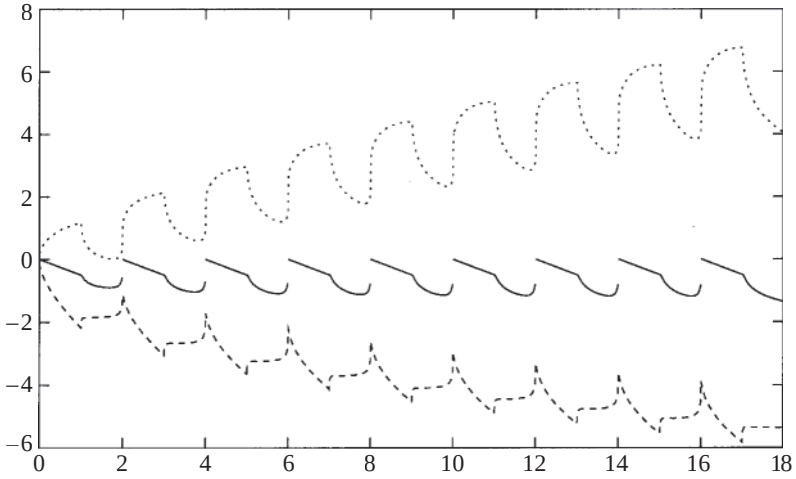

Fig. 9 The wake centre-line shapes and viscous displacements for nine blades at angle of attack. Note the near periodicity in $s(x)$

expand the velocities and pressures *below* the system of blades as

$$v_-(x, y) = v_0^- + \cdots, \qquad p_-(x, y) = \frac{1}{h} p_{-1}^- + p_0^- + \cdots . \tag{5.5a,b}$$

Above the blades the leading-order terms are $O(1)$ in both the pressure and normal velocity but we do not consider these here. Substituting into the Cauchy–Riemann balances yields the leading-order governing equations as $p^-_{-1x} = -v^-_{0y}$, $p^-_{-1y} = 0$. These must be solved subject to the boundary conditions at the underside of the blade, $\hat{y} = 1$, namely $v^-_0(x, 0) = c'(x) - \frac{1}{2}t'(x) - \delta'_-(x)$ on the blades, $v^-_0(x, 0) = s'(x) - \delta'_-(x)$ in the wakes, $p^-_{-1} = 0$ in the wakes.

The velocity conditions here are from (2.5) and we require zero p^-_{-1} in the wake as the leading-order pressure above the blades is $O(1)$ and so for continuity across the wakes the pressure beneath must be zero at this order.

Hence $v^-_{0\hat{y}\hat{y}} = 0$, which we integrate to give $v^-_0 = A(x)\hat{y}$ satisfying the ground condition $v^-_0 = 0$ at $\hat{y} = 0$. The underside conditions lead to $v^-_0 = \big(c'(x) - \frac{1}{2}t'(x) - \delta'_-(x)\big)\hat{y}$, which gives the leading-order pressure underneath blade i as

$$p^-_{-1}(x) = p^-_{-1}(a_i) - c(x) + \tfrac{1}{2}t(x) + \delta_-(x), \tag{5.6}$$

where the constant of integration $p^-_{-1}(a_i)$ is unknown.

This shows that to leading order the pressure is independent of y beneath the blades, that is, $p_- = p_=$, a property which can be clearly seen emerging in the results for small h presented in section 4. Also, for the flat plate case presented in Fig. 3b, $c(x)$ and $t(x)$ are zero and so (5.6) gives the scaled pressure responding as $\delta_-(x)$. Again this can be seen in the pressure plots for the relevant cases in section 4. Perhaps more importantly it shows the pressure beneath the blade system increasing as $1/h$ while that above the system remains $O(1)$, giving an increasingly large pressure difference across the blade and so greatly enhancing any lift or downforce produced. A further feature of interest in the numerical results is the flat shape of the lower displacement function $\delta_-(x)$ in the wakes. This can also be explained here, as in the wakes $p^-_{-1} = 0$ implies $v^-_0 = 0$ with no fluid being entrained to leading order. The wake boundary condition after (5.5b) then implies $s(x) = \delta_-(x) + D$, where D is a constant of integration, and so the graphs showing $s(x) - \delta_-(x)$ would indeed be expected to be flat to leading order.

6. The many-blade limit

The central problem in the many-blade limit is periodic, that of a single blade with leading edge at $x = 0$, trailing edge at $x = t$ and the next leading edge at $x = L$, all at a distance h from horizontal ground. It is assumed that the flow has already come over a large number of identical L -periods upstream of the blade–wake pair of interest and likewise may have a large number still to pass subsequently.

The present results for increasingly many blades, along with the analysis in Smith and Timoshin (**1**, **2**), suggest a two-tiered structure to the flow in the viscous layers. In Figs 10a,b we present the u velocity profiles mid-blade and mid-wake in each relevant period for a representative ten-blade case, obtained as in sections 3, 4. The seemingly periodic nature of the inner tier can be seen in the relatively constant flow for small Y after about three or four blades in each figure but with a changing profile through the period. There is also a slowly growing outer viscous tier, with little change from one blade into the following wake but gradual growth as many blades are passed. These results suggest a two-tiered structure in Y in the viscous layers. In Fig. 10c we compare successive wake centre-line shapes, which again suggest convergence to a periodic state.

After passing over a large number of blades, n say, there are two streamwise length scales of significance: one a longer, slowly varying scale over all the blades passed so far with $x = nx_\ell$, and

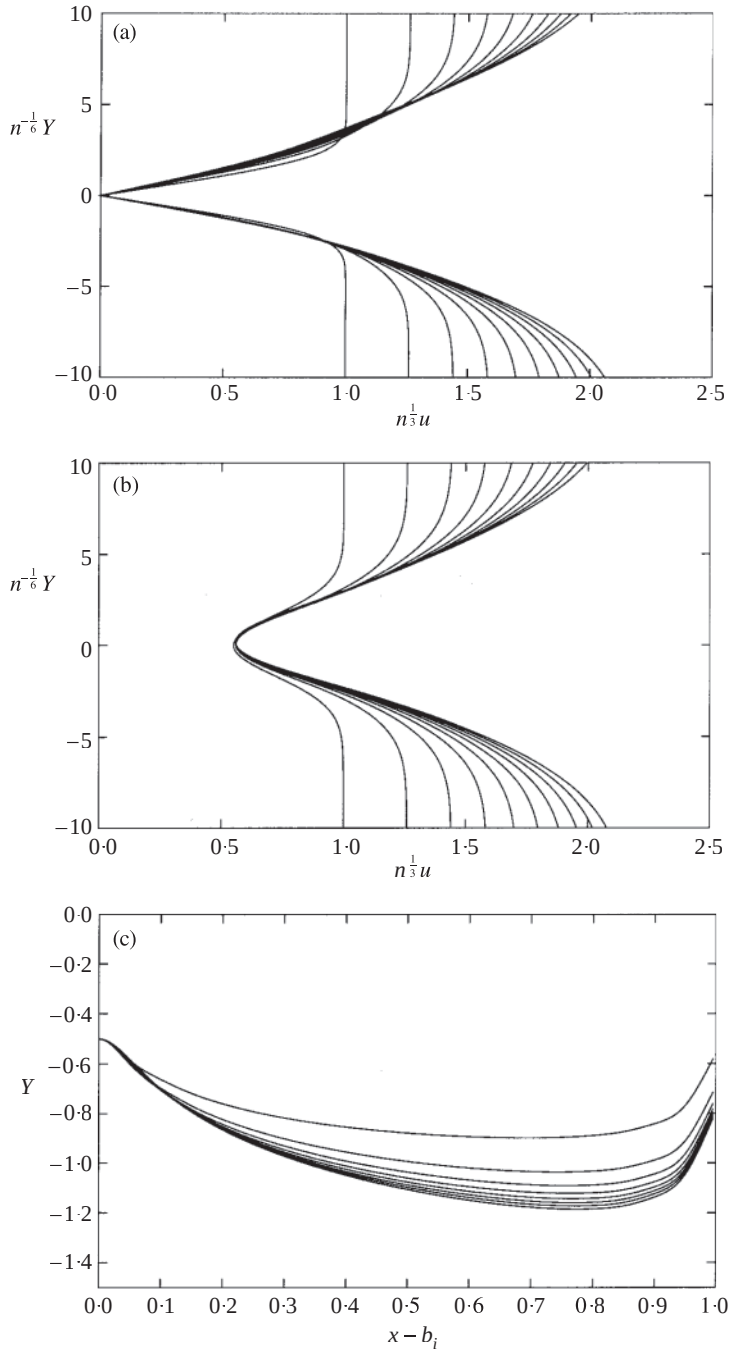

Fig. 10 The scaled u velocity profiles in the viscous layers for a ten-blade case, (a) mid-blade, (b) mid-wake. Note the near periodicity for small y and the gradual growth for large y. The scales used are those determined in section 6 for the innermost layer. (c) Comparison of wake centre-line shapes for successive blades

the other having a fast-varying dependence on the local shifted x of $O(1)$ near the current blade. So we express the x dependence as $x = x_s + nx_\ell$. At a streamwise distance of order n downstream the normal viscous scale is of order $n^{\frac{1}{2}}$ as expected. The normal scaling of the inner tier is implied by the viscous–inviscid balance in the governing equations between $u\partial/\partial x \sim \partial^2/\partial Y^2$ along with the known scalings $x_s \sim O(1)$ and $u \sim O(Yn^{-\frac{1}{2}})$. These imply $Yn^{-\frac{1}{2}} \sim Y^{-2}$ and so give the normal scaling as $Y \sim n^{\frac{1}{6}}$ in the inner tier. Details are discussed in Purvis (**24**), from which we bring out in brief the following points. The bulk of the original viscous layer has primarily mean Blasius flow but sheltered from all the leading and trailing edges by the inner viscous sublayer, and it also serves to communicate displacement effects from the latter through to the outer potential flow region. The sublayer is still governed in essence by (2.1a to c) but now with

$$\partial\bar{u}/\partial Y \to \pm\lambda \quad \text{as} \quad Y \to \pm\infty, \tag{6.1a}$$

$$L - \text{periodicity in } x_s. \tag{6.1b}$$

Here the shear-flow requirement (6.1a) is to match with the bulk motion, where λ [$= 0{\cdot}4696x_L^{-\frac{1}{2}}$] is the scaled Blasius wall shear value, and (6.1b) is the short scale periodicity requirement. The solution determines the sublayer displacement effects $b_\pm(x) = |Y| \mp \bar{u}/\lambda$ at large $|Y|$, which in turn drive the outer inviscid motion and couple with rearrangements due to periodicity applying there.

The viscous problem is thus similar to that in sections 2 to 4 apart from the shear and periodicity requirements (6.1). The solution technique adopted is also much as previously, with the same discretization, changing the $|\tilde{Y}| \to \infty$ condition to satisfy (6.1a) and meeting the periodicity condition by iterating over the L-period until the successive velocity profiles at $x = L$ are identical, to within a reasonable accuracy, to their values on the previous sweep. The problems involved in evaluating the integrals in the inviscid region are largely as before. Overall, given a starting profile, we sweep the viscous-layer solution over the blade and wake period to $x = L$; we then apply the necessary Y-shift calculated from inviscid properties; and this then yields the starting profile for the next sweep if convergence has not been attained. Once converged, the necessary displacements $b_\pm$ can be determined.

We present in Figs 11a,b two comparisons between the periodic solution thus obtained and that of sections 3, 4. The figures show the wake shapes for $h = 0{\cdot}25$ and $h = 0{\cdot}0625$, calculated both by the periodic approach and shown with the fourth wake shape from the five-blade calculations presented in section 4, with $L = 2$ and $t = 1$ in this case. The comparisons add weight to the proposed structure as there is good agreement in both cases, particularly for the smaller-h case where the solution appears to settle into a periodic state far quicker than at large h. Better agreement could probably be achieved by including the next-order displacement effects, but these results appear encouraging with regard to the validity of the three-region structure and the periodicity assumption. In Figs 11c,d we also present comparisons between the pressures beneath the blades at the same heights, comparing this periodic case with the pressure found under blade 4 of the five-blade calculations presented earlier.

7. Final comments

This article has examined the steady planar flow past a number (n) of blades positioned in sequence at an $O(1)$ distance h from the ground. Here h is measured relative to a typical blade chord. Various

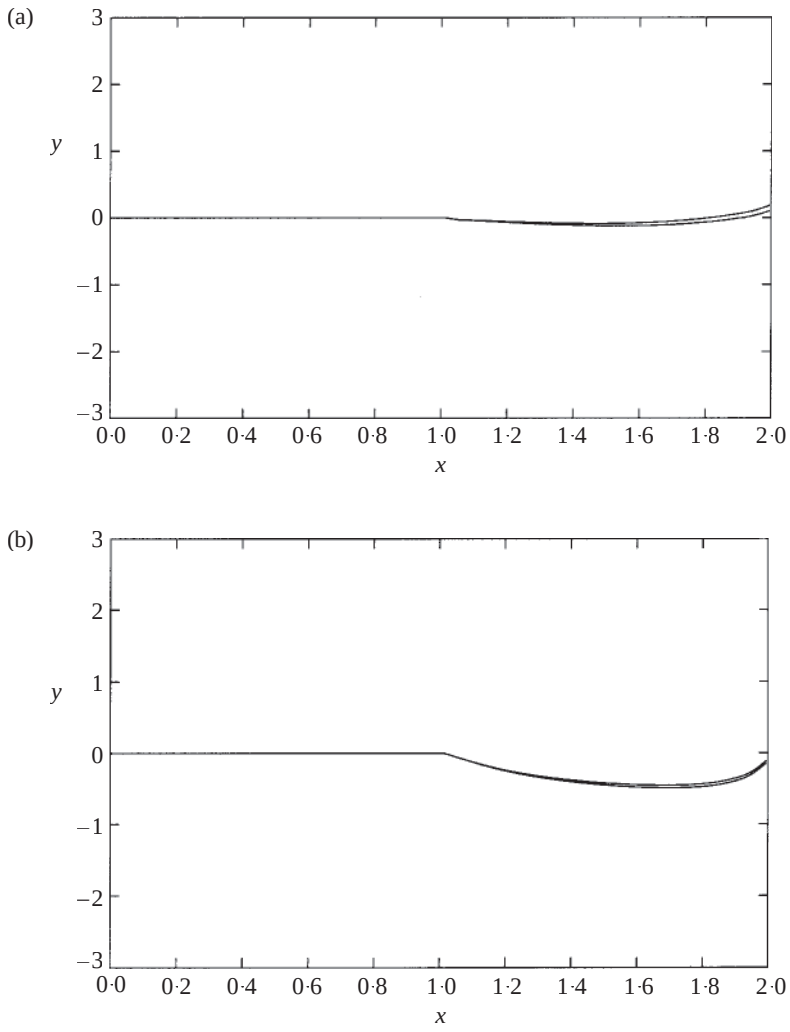

Fig. 11 Comparison between the wake shapes $s(x)$ for the periodic method of section 6 and blade 4 of the five-blade case from section 4, for (a) $h = 0{\cdot}25$, (b) $h = 0{\cdot}0625$. The shape from section 6 is the lower of the two

configurations have been examined, as were two important limits, that of extreme relative ground clearances h (large or small) and the many-blade limit. It is interesting to note that there is almost no change from the large-h case until h is reduced to below about $\frac{1}{2}$; see Figs 3 and 4. As h is reduced further the flow gradually approaches the small-h form which essentially describes the flow for $h < \frac{1}{16}$ in practice. Likewise, for flat blades at a height $h > \frac{1}{2}$, the induced pressure jump is negligibly small and effectively no lift is produced, while for small h the pressure jump, and hence the lift, behave as h^{-1}. It is also worth noting the usefulness of the many-blade limit and

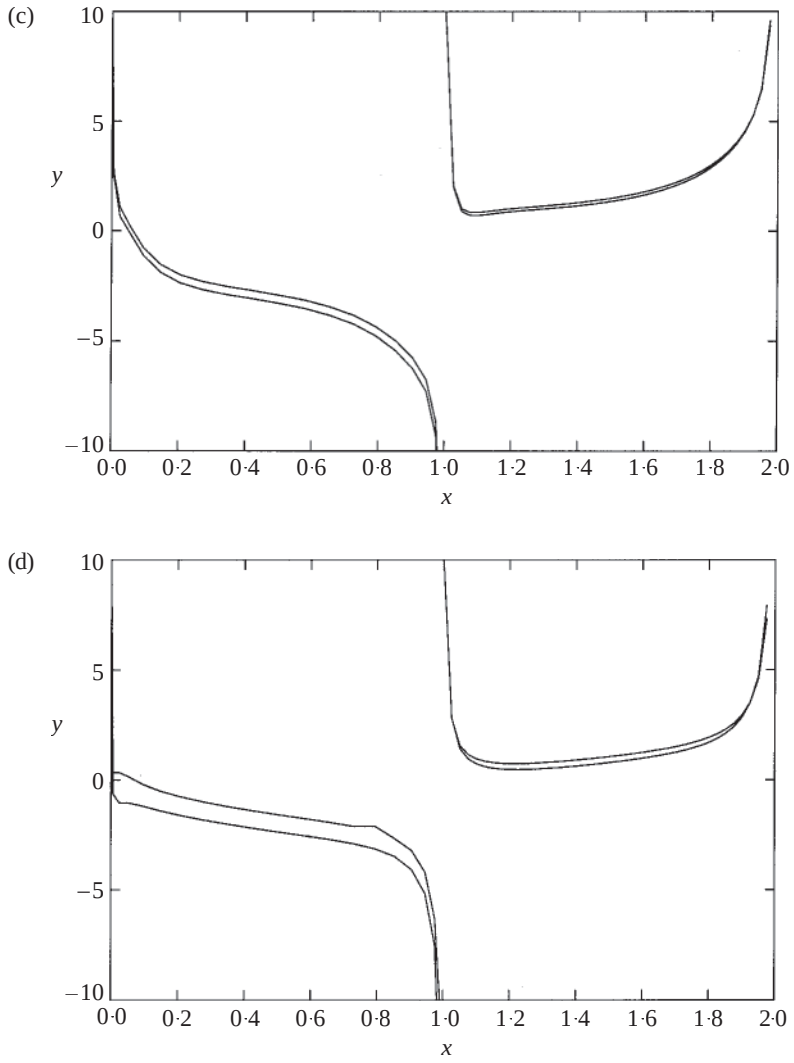

Fig. 11 cont. (c) Comparison between the underneath pressures p^- for the periodic method (lower curves) and for blade 4 of the five-blade case, for $h = 0{\cdot}0625$. (d) As (c) but $h = 0{\cdot}25$

its periodic form. Examining the results suggests that the periodic form is reached after only three or four blades in practice (see Fig. 10 for example). After this the many-blade analysis is found to produce good agreement with further blade features, especially if the next-order displacement terms are included in the calculation. In fact that many-blade work then continues to describe the flow for all subsequent blades until n is very large, of $O(\mathrm{Re}^{\frac{3}{5}})$, after which a new interaction appears with the outer induced pressure becoming comparable in size with the viscous-induced pressure, giving rise

to interactive pressure-displacement problems as in Bowles and Smith (**5**, **6**). This is assuming that the thickness of the viscous layers on the blades and in their wakes, and especially the trailing-edge effect, is insufficiently large to interact directly with the ground. See the interactions in Jones (**4**) and Purvis (**24**).

There are many other aspects which present themselves as follow-up questions to this study. The working is limited so far to blades and gaps of unit length. Investigations into varying the ratio of blade to gap may be of interest, particularly for the case of short blades which physically is closer to a typical rotor-blade setup. Also an investigation into the flow if the blades are not all identical, having varying shapes and/or angles of attack for example, would be of merit, particularly on how the periodic structure develops. Another configuration which warrants attention is that of blades at large angles of attack, when the characteristic wake may no longer encounter the following leading edge. Further enquiry into sheltering effects may also prove fruitful, examining lift, drag and the benefits of slipstreaming.

Of perhaps most importance in technological as well as theoretical terms is the extension to three-dimensional flow, either for a genuine rotating system (see Smith and Timoshin (**1**)) or for three-dimensional blades in a uniform stream similar to the model discussed here. The main difficulty in three dimensions is in solving the outer inviscid problem to feed back into the viscous-layer solution by way of scaled normal shifts, analogous with those in the present study. Non-zero global angles of attack or non-slipstreamed blades also raise difficult issues both with and without ground effect present.

Acknowledgements

Support for the first author from the Engineering and Physical Sciences Research Council is greatfully acknowledged.

References

1. F. T. Smith and S. N. Timoshin, *Proc. R. Soc.* A **452** (1996) 1301–1329.
2. —— and ——, *J. Fluid Mech.* **324** (1996) 355–377.
3. A. T. Conlisk, *Ann. Rev. Fluid Mech.* **29** (1997) 515–567.
4. M. A. Jones, Mechanisms in wing-in-ground-effect aerodynamics. Ph.D. Thesis, University of London (2000).
5. R. G. A. Bowles and F. T. Smith, *Q. Jl Mech. Appl. Math.* **53** (2000) 207–251.
6. —— and ——, *J. Fluid Mech.* **415** (2000) 203–226.
7. S. Bhattacharyya and F. T. Smith, *J. Fluids Engg* (2002) in press.
8. S. Newman, *The Foundations of Helicopter Flight* (Edward Arnold, London 1994).
9. S. E. Widnall and T. M. Barrows, *J. Fluid Mech.* **41** (1970) 769–792.
10. E. O. Tuck and T. M. Bentwich, *ibid* **135** (1983) 51–69.
11. J. Seddon, *Basic Helicopter Dynamics* (BSP Professional Books, Oxford 1990).
12. A. R. S. Bramwell, *Helicopter Dynamics* (Butterworth Heinemann, Oxford 1976).
13. D. W. Moore and P. G. Saffman, *Proc. R. Soc.* A **333** (1973) 491–508.
14. F. X. Caradonna and C. Tung, NASA, TM 81232 (1981).
15. S. P. Parthasarathy, Y. I. Cho and L. H. Back, AIAA paper 85-1557 (1985).
16. D. R. Hoad, S. L. Althoff and J. W. Willot, In *Proc. 44th Ann. Forum Amer. Hel. Soc.* (1988) 57–72.

17. D. R. Hoad, NASA, TP 2946 (1990).
18. P. F. Lorber, *J. Amer. Hel. Soc.* **36** (1991) 66–76.
19. K. W. McAlister, C. A. Schuler, L. Branum and J. C. Wu, NASA, TP 3577 (1995).
20. W. J. McCroskey, AIAA paper 95-0530 (1995).
21. T. A. Egolf and S. P. Sparks, In *Proc. Ann. Forum Amer. Hel. Soc.* (1986) 997–1011.
22. K. Ramachandran, S. Schlechtriem, F. X. Caradonna and J. Steinhoff, *Ann. Forum Amer. Hel. Soc.* (1993) 571–584.
23. G. R. Srinivasan and L. N. Sankar, *Amer. Hel. Soc.*, Specialists meeting on Aeromechanics Tech. and Product Design (1995).
24. R. Purvis, Rotor blades and ground effect. Ph.D. Thesis, University of London (2002).
25. N. I. Muskhelishvili, *Singular Integral Equations*, 2nd edn (Noordhoff, Groningen 1946).